Int. J. Electrochem. Sci., 15 **(2020)** 6330 – 6342, doi: 10.20964/2020.07.20

International Journal of
ELECTROCHEMICAL
SCIENCE
www.electrochemsci.org

Improving Interfacial Problems between the Cathode and Solid-State Electrolyte by Coating ETPTA-PEG onto the Surface of $LiNi_{0.8}Co_{0.1}Mn_{0.1}O_2$

Hongzhi Wang[1], *Yi Bo Shang*[1], *Weiguo Zhang*[1], *Fei Ding*[2,*], *Lin Sang*[2,3]

[1] Department of Applied Chemistry, School of Chemical Engineering and Technology, Tianjin University, Tianjin 300350, PR China
[2] Tianjin Cetc New Energy Research Institute Co., Ltd
[3] National Key Laboratory of Science and Technology on Power Sources, Tianjin
[*]E-mail: hilldingfei@163.com

Received: 3 February 2020 / *Accepted:* 9 April 2020 / *Published:* 10 June 2020

In recent years, the rapid development of the electric vehicle industry has led to the requirement of Li-ion batteries (LIBs) with a higher energy density and better safety. Therefore, solid-state lithium batteries with the above advantages have attracted a lot of attention. However, solving the interfacial problem between cathodes and the solid-state electrolyte has become a major challenge in the practical application of solid-state lithium-ion batteries. In this article, ETPTA (trimethylolpropane ethoxylate triacrylate)-PEG (poly(ethylene glycol)) is introduced onto the surface of $LiNi_{0.8}Co_{0.1}Mn_{0.1}O_2$ cathode materials by ultraviolet irradiation. TEM and FTIR analyses reflect the existence of the composite coating layer. Electrochemical tests reveal that the coated material has better cycle stability (capacity retention remains 84% after 100 cycles), lower interfacial impedance and higher rate capabilities (34 mA h g^{-1} at 2 C). These results reflect the fact that the coating layer plays a significant role in improving the interfacial contact between the cathode and solid-state electrolyte and suppressing surface side reactions.

Keywords: Ni-rich cathode materials, interfacial problem, surface modification

1. INTRODUCTION

Today, the massive consumption of fossil energy and the excessive emission of greenhouse gases has made our environment increasingly worse. According to statistics, nearly 25% of carbon dioxide emissions originate from vehicles running on fossil fuels.[1] To solve this problem, the electric vehicle industry is promoted throughout the world. Almost all electric vehicles currently rely on LIBs;[2] to achieve the requirements of an electric vehicle, LIBs must have a higher energy density, good rate

performance, excellent cycle stability and safety.[3] Replacement of the liquid electrolyte with a solid-state electrolyte is proposed to meet these requirements. In comparison with the traditional liquid electrolyte, the solid-state electrolyte has a higher voltage platform and excellent safety performance; besides, the solid-state electrolyte can suppress the growth of lithium dendrites.[4-6] However, the utilization of the solid-state electrolyte also results in interfacial problems between the electrode and solid-state electrolyte, which has a strong impact on the performance of all-solid-state lithium batteries (ASSLBs).[7] Therefore, ameliorating interfacial problems is the key to promoting the commercialization of ASSLBs.

Interfacial problems include two aspects, on one hand, because point contact is the major way in which contact is made between a cathode and solid-state electrolyte and also because a poor physical contact may occur at the interface during circulation, voids will be created between the cathode and solid-state electrolyte, resulting in increased interfacial resistance, which will greatly affect the performance of ASSLBs.[8] On the other hand, interfacial side reactions can occur at the interface.[9] A wide variety of research has noted that a sudden drop of electric potential (φ) across the interface between the cathode and solid-state electrolyte will promote side reactions; these side reactions will lead to the formation of insulating phases, structural changes in the cathode or decomposition of the solid-state electrolyte;[10,11] besides, these side reactions may consume lithium-ions, causing irreversible capacity loss.[12]

$LiNi_{1-x-y}Co_xMn_yO_2$ (NCM) has attracted wide attention because of its low cost, high operating voltage, and high capacity.[13] However, when a Ni-rich NCM cathode directly contacts the solid-state electrolyte, the volume expansion/shrinkage of the cathode materials upon lithiation/delithiation can make the cathode lose contact with the solid-state electrolyte, which will cause an increase in interfacial resistance.[14] In addition, there is an abundance of Ni^{4+} ions and other metal ions on the surface of Ni-rich NCM cathode materials, which may catalyse some side reactions,[15] causing decomposition of the solid-state electrolyte and the formation of insulating phases at the interface. For example, when using $Li_7La_3Zr_2O_{12}$ (LLZO) as the solid-state electrolyte, LLZO may release oxygen and lithium, which can react with NCM and form an insulating substance.[16] Therefore, it is very important to improve the interfacial problems.

Surface coating is a promising strategy to resolve interfacial problems. Metal oxides (Al_2O_3, TiO_2, MgO),[17-19] fluorides (CoF_2, AlF_3),[20,21] phosphates ($AlPO_4$, Li_3PO_4),[22,23] the solid-state electrolyte ($Li_3xLa_{2/3}$-$xTiO_3$, $Li_{1.3}Al_{0.3}Ti_{1.7}(PO_4)_3$) and conducting polymers (PEO, PANI) have been generally introduced onto the surface of NCM to suppress interfacial side reactions and ameliorate structural stability.[24-27] For example, Choi coated NCM with $Li_{1+x}Al_xTi_{2-x}(PO_4)_3$ (LATP) to improve the lithium-ion conductivity at the interface and protect the cathode from electrolyte attack. After coating, the discharge capacity at 0.1 C increased by approximately 12 mA h g^{-1}; furthermore, the capacity retention remained at 98% after 100 cycles.[28] Zhang used a $Li_3xLa_{2/3}$-$xTiO_3$ (LLTO) coating layer to protect the cathode from being corroded by the electrolyte; the initial coulombic efficiency reached 86.3% with a 7 wt % LLTO coating.[29] Except for inorganic solid-state electrolytes, researchers have also coated NCM with a polymer solid-state electrolyte; for example, Wang coated $LiNi_{0.6}Mn_{0.2}Co_{0.2}O_2$ (NCM622) with poly(acrylonitrile-co-butadiene) to improve the physical contact and electrochemical properties. The coated NCM showed an excellent rate performance; the coated

NCM showed a discharge capacity of 3 C at 99 mA h g^{-1} and still worked at 5 C. In addition, the capacity retention of the coated cathode can reached 75% after 400 cycles at 2 C.[30]

In this paper, we coated NCM with a combination of ETPTA and PEG (2000). Figure 1 shows how the coating layer can improve the interfacial problem between $LiNi_{0.8}Co_{0.1}Mn_{0.1}O_2$ and the solid-state electrolyte. On one hand, how the coating layer can improve the physical contact at the interface due to its softness, which turns a point contact into a surface contact. On the other hand, the coating layer can also suppress interfacial reaction to maintain a low resistance, which has a strong impact on cycle performance. In the composite coating layer, the C=O and –C-O groups in ETPTA can help accelerate the diffusion of Li^+, and also, PEG is a good ionic conductor for the polymer. After coating, the NCM cathode material exhibits a favourable electrochemical performance with a better cycling stability (84% for coated NCM material, 64% for NCM material), lower impedance and improved rate capability (34 mA h g^{-1} at 2 C).

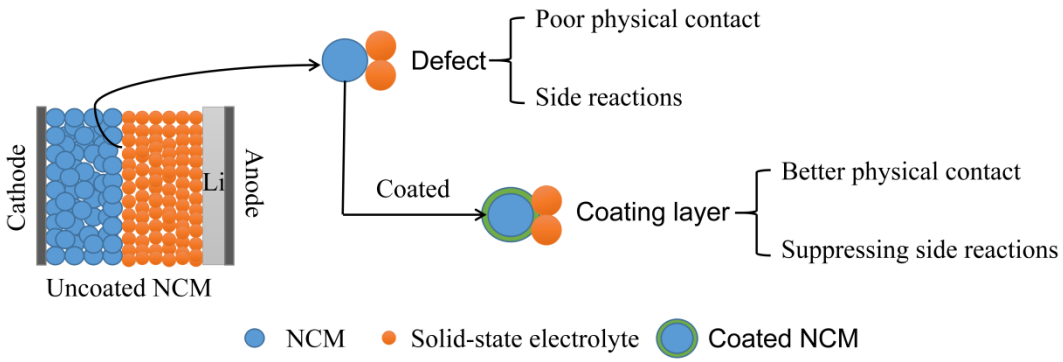

Figure 1. Schematic illustration of interfacial problems and the coating layer to improve the interfacial problem.

2. EXPERIMENTAL SECTION

The pristine material $LiNi_{0.8}Co_{0.1}Mn_{0.1}O_2$ was purchased from Beijing Easpring Material Technology Ltd. Trimethylolpropane ethoxylate triacrylate (ETPTA) and 2-Hydroxy-2-methylpropiophenone (HMPP) was purchased from Aladdin, and PEG (2000) was purchased from Beijing J&K Scientific Ltd.

First, 0.084 g ETPTA and 0.036 g PEG were dissolved in 20 ml 1-methyl-2-pyrrolidinone (NMP) and vigorously stirred for 2 h. Then, 2 g NCM powders and 2 wt % HMPP (related to weight of ETPTA) were added to the solution and vigorously stirred for 6 h to ensure an even dispersion. The solution was then stirred for 2 h under ultraviolet irradiation to obtain the coating layer. Finally, the powders were obtained by vacuum distillation and dried in vacuum for 12 h at 80 ºC.

The morphology and appearance of the samples were investigated by scanning electron microscopy (SEM, Quanta 650 FEG) with an accelerating voltage of 20 kV. The interface situation for the samples was characterized using transmission electron microscopy (TEM,**Tecnai G2 Spirit TWIN**). The X-ray diffraction (XRD) patterns were measured with Cu Kα radiation at a scan speed of 4°min^{-1}.

Fourier transform infrared (FTIR) absorption spectra were recorded in the wavenumber range of 500-4000 cm^{-1} using an FTIR microspectroscopy (Frontier Mid-IR FTIR).

The electrochemical properties were evaluated with CR2040 coin cells assembled in an argon-filled glovebox (H_2O, O_2 < 0.1 ppm). All of the experiments were carried out in all-solid-state cells using metallic lithium as the anode, the NCM@ETPTA-PEG material and NCM material as the cathode, and the PDOL gel electrolyte as the separator and the solid-state electrolyte. The cathode was synthesized by coating a mixture of the active material, super P and polyvinylidene fluoride (PVdF) binder (8:1:1 in weight) in N-methylpyrrolidone (NMP) solvent on Al foil. Then, the working electrodes were dried under vacuum for 12 h at 120 ºC. The active mass loading was approximately 2 mg cm^{-2}. The cells were tested in the voltage range of 2.5-4.3 V versus Li^+/Li using a battery testing system (Land CT2001A, China). Cyclic voltammetry (CV) and electrochemical impedance spectroscopy (EIS) were performed using an electrochemical workstation (CHI660E). All the tests were conducted under room temperature.

3. RESULT AND DISCUSSION

3.1 Structure and composition

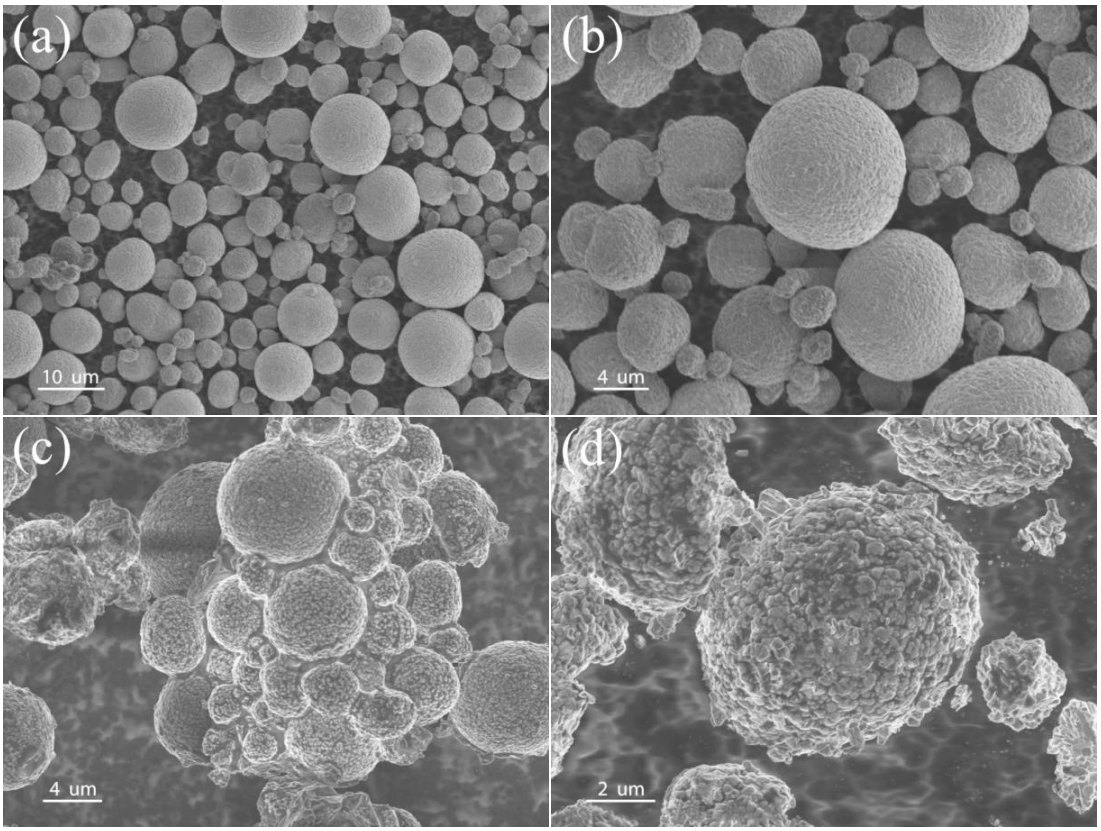

Figure 2. SEM images of (a,b) NCM, (c,d) NCM@ETPTA-PEG samples.

The morphology and appearance of the samples were investigated using SEM measurement. Figure 2a-d shows SEM images of the pristine NCM and NCM@ETPTA-PEG particles with a diameter

of approximately 12 µm. As observed from Figure 2b,d, the pristine NCM and polymer-coated NCM particles were spherical particles consisting of small primary particles, which means that the coating layer did not change the morphology of the pristine material. Compared with the pristine NCM powder, it can be observed in Figure 2c that the surface of NCM@ETPTA−PEG was covered with a continuous film. The existence of a coating layer on the surface of the material was determined by TEM. As shown in Figure 3b, the NCM material is covered with a ETPTA-PEG coating layer, and the thickness of the coating layer is approximately 20-25 nm. By comparison with the pristine NCM material, no lattice fringes for ETPTA-PEG were observed, which indicates that the ETPTA-PEG coating layer was amorphous.

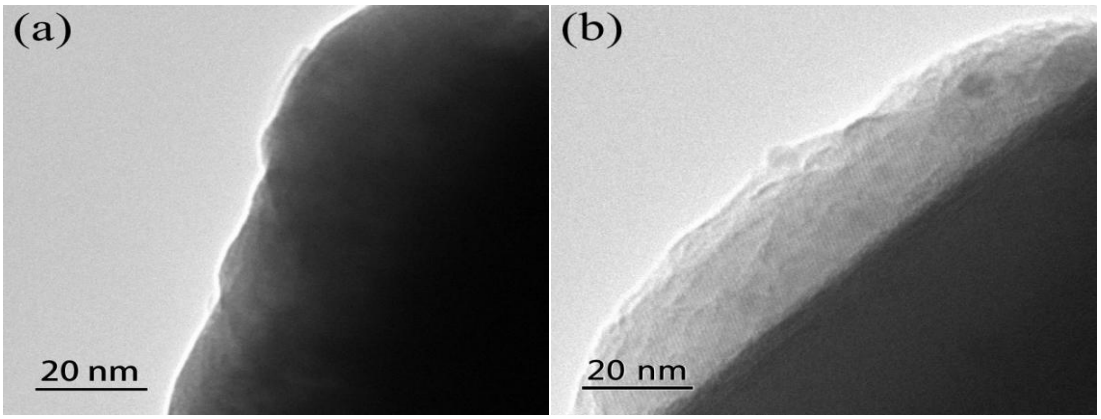

Figure 3. TEM images of (a) NCM, (b) NCM@ETPTA-PEG samples.

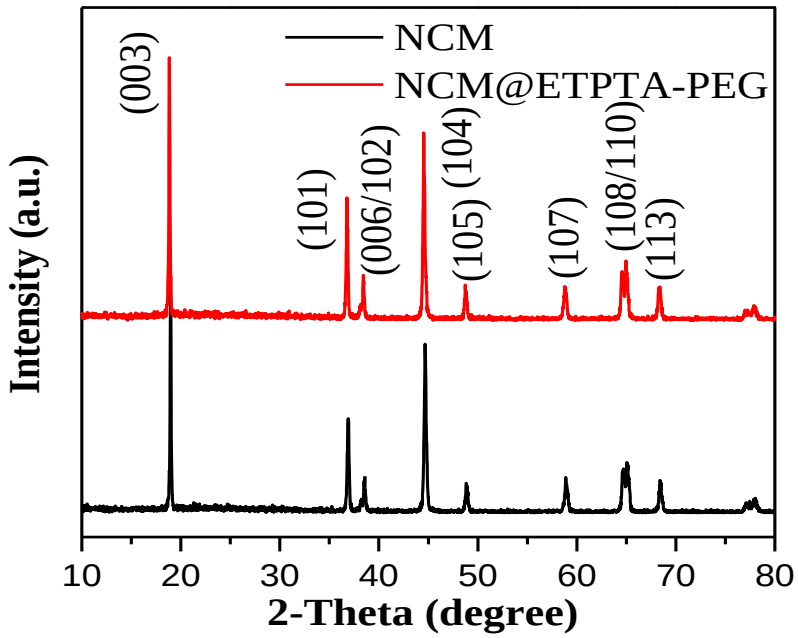

Figure 4. XRD patterns for the NCM and NCM@ETPTA-PEG samples.

The crystal structures of pristine NCM and NCM@ETPTA-PEG were compared using XRD. As observed from Figure 4, the XRD patterns of both samples are all well in accordance with a hexagonal α-NaFeO2 layered structure (R3/m) without the presence of impurities. The clear splitting of the (006)/(102) and (108)/(110) peaks indicate that the samples exhibit a well-ordered crystal structure.[31] In addition, it has been demonstrated that NCM has low cation disorder when the value of I(003)/I(104) > 1.20;[32] in this work, the NCM sample had an I(003)/I(104) value of 1.40, which reflects the fact that the NCM material has a low cation mixed effect. The comparison shown in Figure 4 indicates there are no new diffraction peaks exhibit in the pattern measured for NCM@ETPTA-PEG, which means that the ETPTA-PEG coating layer is amorphous. These results confirm that the surface treatment of NCM with ETPTA-PEG has no obvious effect on the crystal structure of pristine NCM material.

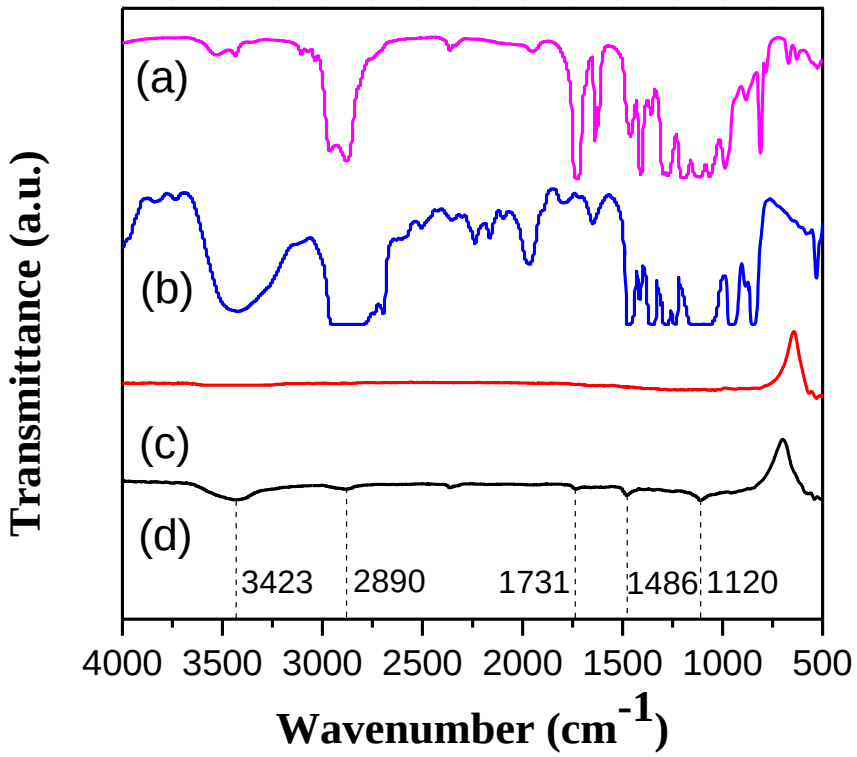

Figure 5. FTIR spectra for the (a) ETPTA, (b) PEG, (c) NCM, (d)NCM@ETPTA-PEG samples.

FTIR was applied to confirm the presence of the ETPTA-PEG coating layer on the surface of NCM. Figure 5 displays the FTIR results for (a) ETPTA, (b) PEG, (c) NCM, (d) NCM@ETPTA-PEG. Compared with ETPTA monomers, the peak at 1731 cm^{-1} and the disappearance of the C=C stretching vibration (in the range of 1610-1680 cm^{-1}) in the spectra for NCM@ETPTA-PEG confirm monomers complete polymeriziation and the existence of ETPTA.[33] In addition, the typical peaks at 1120 cm^{-1} can be attributed to the stretching vibration of -C-O in O=C-O groups. According to a previous report, -C-O and C=O groups can help accelerate the diffusion of Li^+.[34] The stretching vibration of $-CH_2--CH_2-$ and the stretching vibration of OH^- in PEG are confirmed by the observation of peaks

located at 1486 cm^{-1}, 2890 cm^{-1}, and 3423 cm^{-1}. These results demonstrated that the NCM material was coated by ETPTA−PEG polymers (the FTIR spectra for NCM and NCM@ETPTA-PEG is also shown in Figure S1).

3.2 Electrochemical properties

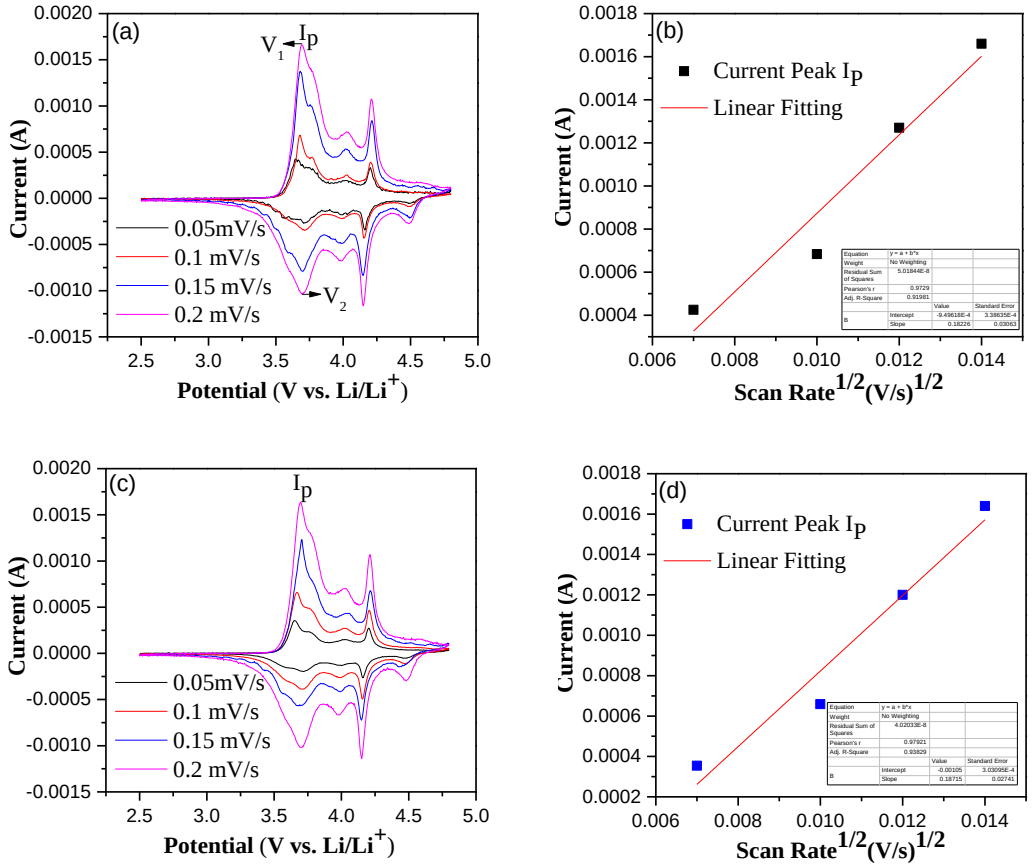

Figure 6. CV profiles for (a) NCM and (c) NCM@ETPTA-PEG; (b) and (d) are the corresponding linear fitting

To study the electrochemical performance and lithium transfer kinetics, cyclic voltammetry (CV) was tested within the voltage range of 2.5-4.8 V at different scan rates. Figure 6a,b shows that the CV curves for both samples include three pairs of redox peaks, indicating that the cathode undergoes a series of phase transitions, which can be expressed as from hexagonal to monoclinic ($H_1 \leftrightarrow M$), monoclinic to hexagonal ($M \leftrightarrow H_2$) and hexagonal to hexagonal ($H_2 \leftrightarrow H_3$) during the charge and discharge process. As is known, the corresponding potential difference ($\Delta V = V_1 - V_2$) between the oxidation peak and reduction peak is related to the reversibility of the cyclic process;[35] the ΔV values for NCM and NCM@ETPTA-PEG were 6.28×10^{-3} V and 2.77×10^{-3} V, respectively. The low ΔV for NCM@ETPTA-PEG indicates that the coating layer can reduce the polarization of NCM. Figure 6a,c shows the CV for NCM and

NCM@ETPTA-PEG at different scan rates. The CV profiles at different scan rates can be used to obtain the diffusion coefficients for Li^+ by using the Randles–Sevcik equation:[36]

$$I_p = 2.69\times10^5 n^{\frac{3}{2}} A D^{\frac{1}{2}} C v^{\frac{1}{2}}$$

where Ip is the peak current intensity (A) of the CV profiles, n is the number of electrons involved in the redox reactions, D is the diffusion coefficient of the lithium ions ($cm^2\ S^{-1}$), C ($C=n/N_a/V$) is the concentration of lithium ions in NCM material (mol cm^{-3}), and ν is the scan rate (V s^{-1}).

The linear relationships between I_p (A) and the square root of ν (V s^{-1}) is shown in Figure 6c,d (the form in the profiles of the corresponding linear fitting curves is shown in Figure S2) and the Li^+ diffusion coefficients for NCM and NCM@ETPTA-PEG are calculated to be 9.352×10^{-10} and 9.861×10^{-10}, respectively, with little difference in Li+ diffusion. The possible reasons for the improved diffusion coefficients can be ascribed to the suppression of surface side reactions and improved physical contact due to the use of the coating layer. The result from the CV test indicated that the ETPTA-PEG coating layer has a positive impact on enhancing the electrochemical performance of the NCM material.

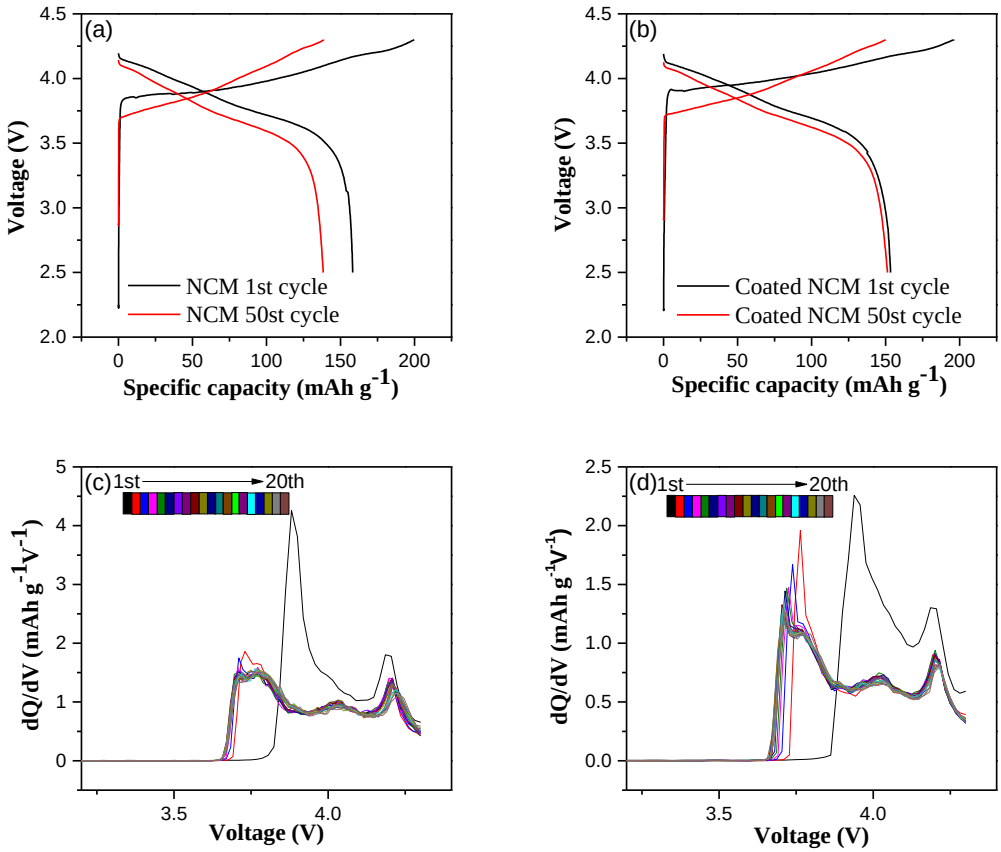

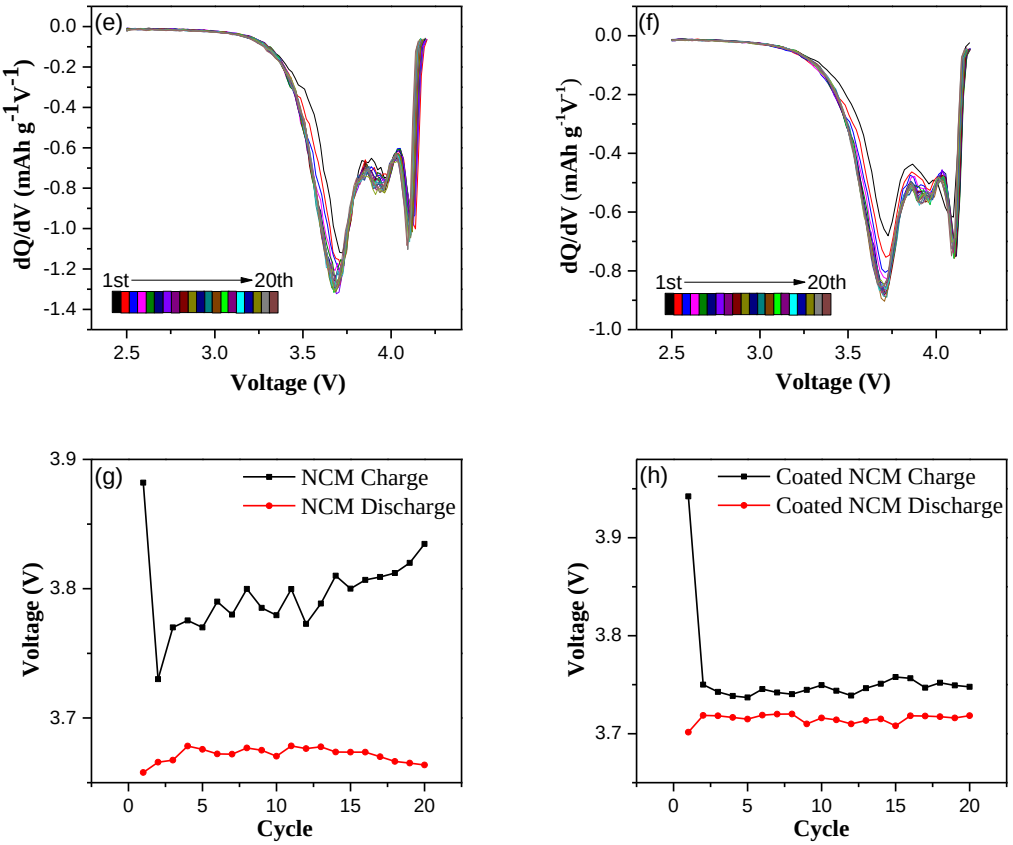

Figure 7. Charge/discharge profiles for (a) NCM and (b) NCM@ETPTA-PEG. The dQ/dV profiles for (c,e) NCM and (d,f) NCM@ETPTA-PEG in the first twenty cycles. Redox peaks for (g) NCM and (h) NCM@ETPTA-PEG in the first twenty cycles.

A galvanostatic charge/discharge measurement was employed to study the electrochemical performance of samples. All the cells were tested at 0.2 C (1 C=200 mA h g^{-1}) within the voltage range of 2.5-4.3 V. Figure 7a,b shows that the initial discharge capacities of uncoated NCM and coated NCM were 158.6 mA h g^{-1} and 154.1 mA h g^{-1}, respectively.

The decreased amount of discharge capacity is ascribed to the inactive coating material; although the initial discharge capacity of coated NCM is lower than that of the uncoated NCM, the Coulomb efficiency of the coated NCM is high (uncoated NCM=78%, coated NCM=80%); the discharge capacity of uncoated NCM and coated NCM after 50 cycles was 138.4 mA h g^{-1} and 151.3 mA h g^{-1}, respectively. According to a previous report,[1] the decrease in coulomb efficiency in the first cycle is mainly due to interface side reactions, which may consume lithium-ions and cause an irreversible capacity loss; therefore, this result indicates that the ETPTA-PEG coating layer helps suppress the interface side reaction, thereby decreasing the loss of initial irreversible capacity. As is shown in Figure 7c-f, the dQ/dV profiles for the first 20 cycles display a variation in potential peaks.

The redox potentials for the first 20 cycles are shown in Figure 7g,h. Except for the first oxidation and reduction potentials, the oxidation potential of pristine NCM increases due to the increasing electrochemical polarization as the cycle progresses. Compared with pristine NCM, the oxidation

potential of the NCM@ETPTA-PEG cathode decreases from 3.94 V to 3.75 V during the first to twentieth cycle. For the trends of the reduction potentials for NCM and NCM@ETPTA-PEG during the cyclic process, although there is no obvious difference between them, the reduction potential of the coated material is higher than that of the uncoated material. The reduction potential of NCM@ETPTA-PEG and pristine NCM was 3.71 V and 3.66 V, respectively. The difference in the redox potential of NCM and NCM@ETPTA-PEG reveals the change in the voltage polarization during the cycles, which can indicate that the ETPTA-PEG coating layer can contribute to the decrease in polarization and maintain it at a low level; these results are in accordance with the CV tests.

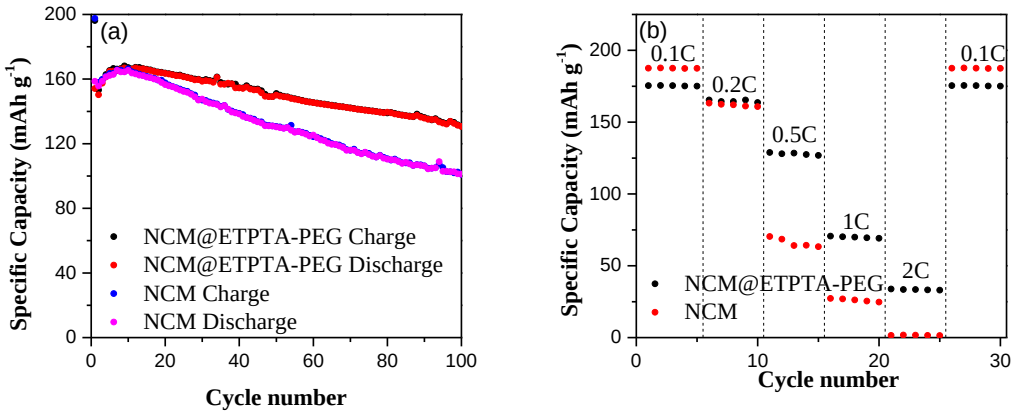

Figure 8. (a)Cycle performance of NCM and NCM@ETPTA-PEG under 0.2C. Rate performance of (b) NCM and NCM@ETPTA-PEG at different current densities.

The cycling performance is shown in Figure 8a. The capacity retention for coated NCM reached 84% after 100 cycles (130.7 mA h g^{-1}), while the capacity retention for uncoated NCM remained at only 64% (101.2 mA h g^{-1}). According to previous reports,[37,38] the side reactions are highly associated with capacity degradation and irreversible phase transformation during the cycling process. Therefore, the ETPTA-PEG coating layer effectively inhibits the side reactions at the interface and the irreversible structural transformation of NCM. The rate performance of the samples was investigated at 0.1 C, 0.2 C, 0.5 C, 1 C and 2 C in the voltage range of 3.0-4.3 V. It can be clearly observed from Figure 8b that the discharge specific capacity of uncoated NCM and coated NCM are similar under low rates (0.1, 0.2 C); however, the discharge specific capacity of uncoated NCM decreases significantly as the rate increases, it delivering 64.3 mA h g^{-1}, 26.5 mA h g^{-1} and 1.5 mA h g^{-1} at 0.5 C, 1 C and 2 C, respectively. In contrast, for varying rates from 0.5 C to 2 C, the discharge specific capacity of coated NCM changes from 128.4 mA h g^{-1} to 34.2 mA h g^{-1}. The significant improvement in the rate performance suggests that the ETPTA-PEG coating layer can accelerate Li-ion diffusion and maintain structure stability, which is in accordance with the previous discussion.

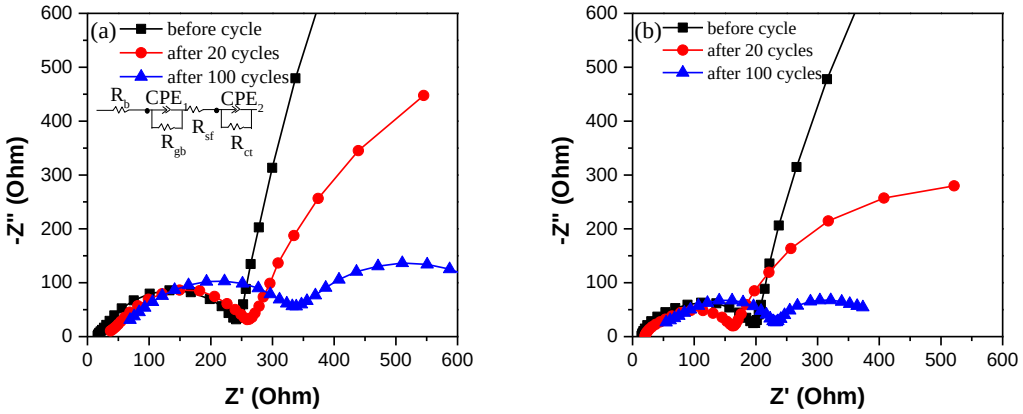

Figure 9. EIS plots for the (a) NCM and (b) NCM@ETPTA-PEG electrodes.

EIS was applied to investigate the interfacial properties of NCM and NCM@ETPTA-PEG at different intervals during cycling. The EIS results fitted by the equivalent circuit are summarized in the Figure 9, where R_b represents the resistance of the bulk of the solid-state electrolyte, R_{gb} represents the resistance of the grain boundary of the solid-state electrolyte, R_{sf} represents the resistance of the interface between the cathode and solid-state electrolyte, R_{ct} represents the resistance of the cathode, CPE_1 represents the constant phase elements originating from the grain boundaries of the solid-state electrolyte, and CPE_2 represents the constant phase elements originating from the cathode. Each plot is composed of a straight line and a semicircle. As seen from Figure 9, R_{sf} for the NCM@ETPTA-PEG is lower than that for the pristine NCM material throughout the cycling, which indicates that the ETPTA-PEG coating layer can improve the physical contact at the interface. Before cycling, R_{ct} for the uncoated material and coated material is 183.9 Ω and 164.3 Ω, respectively. After 20 cycles, R_{ct} for the uncoated material increases to 205.2 Ω, and R_{ct} for the coated material decreases to 153.4 Ω, in accordance with previous reports,[30,39,40] which suggests that the coating layer is helpful in inhibiting the interfacial side reaction and improving the physical contact between the solid-state electrolyte and cathode. As the cycle progresses, R_{ct} for both materials increases, but R_{ct} of the coated material(177.4 Ω after 100 cycles) is always lower than that for the uncoated material(272.8 Ω after 100 cycles). The EIS results demonstrate that the ETPTA-PEG coating layer can improve the physical contact between the solid-state electrolyte and cathode and inhibit the interfacial side reaction, which leads to the maintenance of lower interfacial resistance; these results are consistent with previous electrochemical test results.

4. CONCLUSIONS

In summary, a composite coating layer was introduced onto the surface of $LiNi_{0.8}Co_{0.1}Mn_{0.1}O_2$ by ultraviolet irradiation that can ameliorate the interfacial problems incurred during the charging-discharging process. Electrochemical tests show that the coated NCM material has a better cycle stability (84% capacity retention after 100 cycles), lower interfacial impedance, and higher rate capabilities (70.5

mA h g^{-1} at 1 C, 34.2 mA h g^{-1} at 2 C) than pristine NCM material. These results illustrate the fact that the composite coating layer helps suppress surface side reactions and improves physical contact at the interface. Therefore, the simple strategy of surface modification presented in this work may be a promising strategy to enhance the electrochemical performance of Ni-rich cathode materials, which can promote the practical application of solid-state lithium batteries.

ACKNOWLEDGEMENTS
This work was financially supported by the National Key Laboratory of Science and Technology at the Power Sources of Tianjin CETC. The authors thank all the people who made efforts towards or were concerned about this work.

References

1. K. Raimund, A. Isabel, D. Christian, L. Thomas, W. Zhang, B.O. Jan, H. Pascal, Z.G. Wolfgang and J. Jürgen, *Chem. Mater.*, 29 (2017) 5574.
2. J. Zheng, T. Liu, Z. Hu, Y. Wei, X. Song, Y. Ren, W. Wang, M. Rao, Y. Lin, Z. Chen, J. Lu, C. Wang, K. Amine and F. Pan, *J. Am. Chem. Soc.*, 138 (2016) 13326.
3. K.S. Kang, Y.S. Meng, J. Breger, C.P. Grey and G. Ceder, *Science*, 311 (2006) 977.
4. H. Duan, Y.X. Yin, Y. Shi, P.F. Wang, X.D. Zhang, C.P. Yang, J.L. Shi, R. Wen, Y.G. Guo and J. Wan, *J. Am. Chem. Soc.*, 140 (2017) 82.
5. J. Janek, W.G. Zeier, *Nat. Energy*, 1 (2016) 16141.
6. R. Xu, X.Q. Zhang, X.B. Cheng, H.J. Peng, C.Z. Zhao, Y. Chong and J.Q. Huang, *Adv. Funct. Mater.*, 28 (2018) 1870049.
7. Y. Yamakawa, S. Hayashi and A. Tatsumisago, *J. Mater. Chem.*, 5 (2017) 10658.
8. J. Wakasugi, H. Munakata and K. Kanamura, *Electrochemistry*, 85 (2017) 77.
9. R. Koerver, F. Walther, I. Ayguen, J. Sann, C. Dietrich, W.G. Zeier and J. Janek, *J. Mater. Chem.*, 5 (2017) 22750.
10. W.D. Zhou, S.F. Wang, Y.T. Li, S. Xin, A. Manthiram and J.B. Goodenough, *J. Am. Chem. Soc.*, 138 (2016) 9385.
11. L. Miara, A. Windmüller, C.L. Tsai, W.D. Richards, Q. Ma, S. Uhlenbruck, O. Guillon and G. Ceder, *ACS Appl. Mater. Interfaces*, 8 (2016) 26842.
12. S. Han, B. Qiu, Z. Wei, Y. Xia and Z. Liu, *J. Power Sources*, 268 (2014) 683.
13. F. Lin, I. Markus, D. Nordlund, T.C. Weng, M. Asta, H.L. Xin and M.M. Doeff, *Nat. Commun.*, 5 (2014) 3529.
14. C. Sun, J. Liu, Y. Gong, D.P. Wilkinson and J. Zhang, *Nano Energy*, 33 (2017) 363.
15. J. Liao, A. Manthiram, *J. Power Sources*, 282 (2015) 429.
16. R. Koerver, I. Aygun, T. Leichtweiss, C. Dietrich, W.B. Zhang, J.O. Binder, P. Hartmann, W.G. Zeier and J. Janek, *Chem. Mater.*, 29 (2017) 5574.
17. F. Wu, N. Li, Y. Su, H. Lu, L. Zhang, R. An, Z. Wang, L. Bao and S. Chen, *J. Mater. Chem.*, 22 (2012) 1489.
18. J. Zheng, J. Li, Z. Zhang, X. Guo and Y. Yang, *Solid State Ionics*, 179 (2008) 1794.
19. S. Shi, J. Tu, Y. Tang, X. Liu, Y. Zhang, X. Wang and C. Gu, *Electrochim. Acta*, 88 (2013) 671.
20. S. Chong, Y. Chen, W. Yan, S. Guo, Q. Tan, Y. Wu, T. Jiang and Y. Liu, *J. Power Sources*, 332 (2016) 230.
21. G. Li, X. Feng, Y. Ding, S. Ye and X. Gao, *Electrochim. Acta*, 78 (2012) 308.
22. F. Wu, X. Zhang, T. Zhao, L. Li, M. Xie and R. Chen, *ACS Appl. Mater. Interfaces*, 7 (2015) 3773.
23. M. Wang, R. Zhang, Y. Gong, Y. Su, D. Xiang, L. Chen, Y. Chen, M. Luo and M. Chu, *Solid State*

Ionics, 312 (2017) 53.
24. D. Cho, H. Yashiro, Y. Sun and S.T. Myung, *J. Electrochem. Soc.*, 161 (2014) 142.
25. Y. Cao, X. Qi, Y. Wang, K. Hu, Z. Gan, Y. Li, G. Hu, Z. Peng and K. Du, *ACS Appl. Mater. Interfaces*, 10 (2018) 18270.
26. C. Yang, P. Liao, Y. Wu and S. Lue, *Appl. Surf. Sci.*, 399 (2017) 670.
27. J. Liang, X. Zeng, X. Zhang, P. Wang, J. Ma, Y. Yin, X. Wu, Y. Guo and L. Wan, *J. Am Chem Soc.*, 140 (22) 6767.
28. J.W. Choi, J.W. Lee, *J. Power Sources*, 307 (2016) 63.
29. H. Zhang, T. Yang, Y. Han, D. Song, X. Shi, L. Zhang and L. Bie, *J. Power Sources*, 364 (2017) 272.
30. L. Wang, X. Zhang, T. Wang, Y. Yin, J. Shi, C. Wang and Y. Guo, *Adv. Energy Mater.*, 24 (2018) 1528.
31. C. Shen, Q. Wang, F. Fu, L. Huang, Z. Lin, S. Shen, H. Su, X. Zheng, B. Xu, J. Li and S. Sun, *ACS Appl. Mater. Interfaces*, 6 (2014) 5516.
32. T. Ohzuku, *J. Electrochem, Soc.*, 140 (1993) 1862.
33. X. Zhang, S. Zhao, J. Wang, W. Fan and C. Li, *Electrochim. Acta*, 301 (2019) 304.
34. H. Duan, Y. Yin, X. Zeng, J. Li, J. Shi, Y. Shi, R. Wen, Y. Guo and L. Wan, *Energy Storage Mater.*, 10 (2018) 85.
35. Q. Gan, N. Qin, Y. Zhu, Z. Huang, F. Zhang, S. Gu, J. Xie, K. Zhang, L. Lu and Z. Lu, *ACS Appl. Mater. Interfaces*, 13 (2019) 12594.
36. Z. Chen, D.L. Chao, J.L. Liu, M. Copley, J.Y. Lin, Z.X. Shen, G.T. Kim and S. Passerini, *J. Mater. Chem.*, 5 (2017) 15669.
37. Z. Chen, D. Chao, J. Lin and Z. Shen, *Mater. Res. Bull.*, 96 (2017) 491.
38. Y. Ding, R. Wang, L. Wang, K. Cheng, Z. Zhao, D. Mu and B. Wu, *Energy Procedia*, 105 (2017) 2941.
39. S. Kobylianska, D. Demchuk, V. Khomenko, V. Barsukov and A. Belous, *J. Electrochem. Soc.*, 166 (2019) 1920.
40. T. Liu, Y. Zhang, X. Zhang, L. Wang, S. Zhao, Y. Lin, Y. Shen, J. Luo, L. Li and C. Nan, *Journal of Materials Chemistry A*, 6 (2018) 4649.

© 2020 The Authors. Published by ESG (www.electrochemsci.org). This article is an open access article distributed under the terms and conditions of the Creative Commons Attribution license (http://creativecommons.org/licenses/by/4.0/).